HHS Public Access

Author manuscript

*ACS Appl Mater Interfaces*. Author manuscript; available in PMC 2020 May 01.

Published in final edited form as:

*ACS Appl Mater Interfaces*. 2019 May 01; 11(17): 15316–15321. doi:10.1021/acsami.9b02750.

# Assessment of Targeted Nanoparticle Assemblies for Atherosclerosis Imaging with Positron Emission Tomography and Potential for Clinical Translation

**Yongjian Liu**[*,†], **Hannah P. Luehmann**[†], **Lisa Detering**[†], **Eric D. Pressly**[§], **Alaina J. McGrath**[§], **Deborah Sultan**[†], **Annie Nguyen**[‡], **Susannah Grathwohl**[‡], **Monica Shokeen**[†], **Mohamed Zayed**[⊥], **Robert J. Gropler**[†], **Dana Abendschein**[‡], **Craig J. Hawker**[§], **Pamela K. Woodard**[*,†]

[†]Mallinckrodt Institute of Radiology, Washington University, St. Louis, Missouri 63110, United States

[⊥]Department of Surgery, Washington University, St. Louis, Missouri 63110, United States

[‡]Department of Medicine, Washington University, St. Louis, Missouri 63110, United States

[§]Materials Department, University of California, Santa Barbara, California 93106, United States

## Abstract

Nanoparticles have been assessed in preclinical models of atherosclerosis for detection of plaque complexity and treatment. However, their successful clinical translation has been hampered by less than satisfactory plaque detection, and lack of a general strategy for assessing the translational potential of nanoparticles. Herein, nanoparticles based on comb-copolymer assemblies were synthesized through a modular construction approach with precise control over the conjugation of multiple functional building blocks for *in vivo* evaluation. This high level of design control also allows physicochemical properties to be varied in a controllable fashion. Through conjugation of c-atrial natriuretic factor (CANF) peptide and radiolabeling with $^{64}$Cu, the $^{64}$Cu-CANF-Comb nanoparticle was assessed for plaque imaging by targeting natriuretic peptide clearance receptor (NPRC) in a double-injury atherosclerosis model in rabbits. The extended blood circulation and improved binding capacity of $^{64}$Cu-CANF-Comb nanoparticles afforded sensitive and specific detection of NPRC upregulated in atherosclerotic lesions by positron emission tomography (PET) at intervals during the progression of disease. Ex vivo tissue validation using autoradiography and immunostaining on human carotid endarterectomy specimens demonstrated specific binding of $^{64}$Cu-CANF-Comb to human NPRC receptors. Taken together, this study not only shows the potential of NPRC-targeted $^{64}$Cu-CANF-Comb nanoparticles for increased sensitivity to an epitope that increases during atherosclerosis plaque development, but also provides a useful strategy for the general design and assessment of translational potential of nanoparticles in cardiovascular imaging.

[*] yongjianliu@wustl.edu; woodardp@wustl.edu.

**Supporting Information**.

The Supporting Information is available free of charge on the ACS Publications website.

Additional experimental data (PDF)

The authors declare no conflict of interest.

## Graphical Abstract

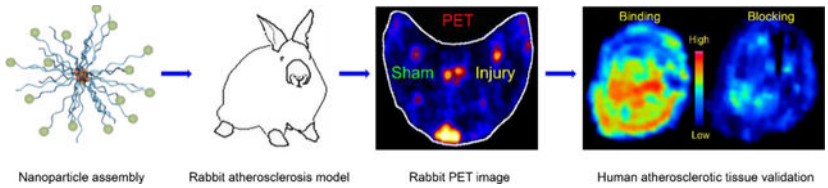


$^{64}$Cu-CANF-comb nanoparticles were synthesized by a modular approach for sensitive and specific PET imaging of natriuretic peptide clearance receptor on complex arterial plaques in a rabbit atherosclerosis model and validation in human carotid endarterectomy specimens. This study illustrates a general strategy for assessing the translational potential of nanoparticle probes for detection of atherosclerosis complexity.

### Keywords

Nanoparticle; NPRC; atherosclerosis; positron emission tomography; translation

Atherosclerosis, the leading cause of morbidity and mortality in Westernized societies, is a progressive disease characterized by the development of lipid-rich plaque lesions within vessel walls and extending into the vascular lumen. It is the underlying basis of cardiovascular diseases including myocardial infarction, stroke, and peripheral arterial disease.[1–4] Due to the chronic nature and long asymptomatic phase, the clinical challenge of atherosclerosis is predicting when a plaque may cause vessel occlusion and associated management of treatment to avoid fatal consequences.[5] Despite major advances in risk factor modification, anatomic imaging tools, new therapeutics, and revascularization techniques, by 2030, the prevalence of atherosclerotic heart disease and its complications are not only projected to increase by 12%,[6] but also result in a significant financial burden.[6]

Complex plaque pathophysiology results from the dynamic expression and often low abundance of disease-related targets on advanced plaques, a scenario that limits clinically available anatomic imaging modalities from reliably visualizing specific cellular features or biological processes that identify high-risk individuals for targeted treatment. Thus, the ability to detect plaques using nanoscale probes is playing an increasingly important role in diagnosis and drug discovery for cardiovascular diseases.[5, 7–9] Of various imaging modalities, radionuclide-based molecular imaging, especially positron emission tomography (PET), has been widely exploited for atherosclerosis diagnosis due to its high sensitivity, quantification, functional detection, non-invasive nature, and well-established pathways for human translation.[10–12] Compared to small molecules or peptide-based imaging platforms with rapid *in vivo* pharmacokinetics, nanoparticles provide unique advantages for atherosclerosis imaging and therapy including extended blood circulation, improved sensitivity and specificity, and elevated drug loading capacity for theranostics.[13–19]

Previously, we reported a polymeric nanoparticle ($^{64}$Cu-CANF-Comb) for targeted PET imaging of natriuretic peptide clearance receptor (NPRC) that is overexpressed on atherosclerotic lesions in a mouse apoE knock-out (apoE$^{-/-}$) model.[20] Due to the modular

design and construction of this polymeric nanoparticle that enables large-scale and stringently-controlled synthesis for translational studies, we wanted to further assess this nanoprobe for plaque imaging in rabbits with advanced atherosclerosis.[21] Moreover, based on our previous report showing up-regulation of NPRC receptor in the intima of advanced atherosclerotic lesions in the carotid arteries of patients who underwent carotid endarterectomy (CEA),[22] we characterized the binding profile of $^{64}$Cu-CANF-Comb to human NPRC receptors expressed on CEA specimens using *ex vivo* autoradiography. We hypothesized that the combination of an advanced preclinical model and human CEA specimens would be a useful strategy to assess the potential of $^{64}$Cu-CANF-Comb and other agents for future assessment of atherosclerosis severity in patients using PET imaging.

## RESULTS AND DISCUSSION

### Synthesis of CANF-Comb nanoparticle

The CANF-Comb nanoparticle was synthesized by adopting the modular strategy previously developed, where precise control over the number and location of CANF in the final assembled structure could be accomplished.[20] We first prepared the functional methacrylate-based monomers: PEG-methacrylate (PEGMA), CANF-PEG-methacrylate (CANF-PEGMA), and DOTA-methacrylate (DOTA-MA). These functional monomers were randomly copolymerized with methyl methacrylate *via* reversible RAFT polymerization to achieve the amphiphilic comb copolymer depicted in Figure 1a. By using a controlled radical polymerization technique, the feed ratio of the functional monomers dictated the ratio incorporated into the final copolymer, affording desirable physicochemical properties and targeting capability of the final CANF-Comb nanoparticles after assembly. As shown in Table 1, the targeted CANF-Comb nanoparticle has ~35 copies of CANF peptide on the surface for NPRC receptor targeting and ~105 copies of DOTA chelator buried in the core for $^{64}$Cu radiolabeling.

### PET imaging in rabbit atherosclerosis model

At 4 weeks after air desiccation-induced injury of the femoral arteries in hypercholesterolemic rabbits, PET imaging at 24 h post-injection of $^{64}$Cu-CANF-Comb showed significant uptake in the injured artery with minimal signal observed in the sham-operated artery (Figure 2). Quantitative uptake analysis showed that the SUV of $^{64}$Cu-CANF-Comb at the injury site was 4.93±0.98 (n=12), which was 2.5 times as much as that determined from the sham site (1.96 ± 0.66, n=12, $p < 0.001$). A competitive receptor blocking study, using an excess amount of non-radiolabeled CANF-Comb, resulted in more than 50% decrease of $^{64}$Cu-CANF-Comb uptake at the injured site (2.36 ± 0.62, n=4) to a level not significantly different from the sham artery (1.53± 0.21, n=4) (Figure 2E, G), demonstrating the plaque targeting specificity of $^{64}$Cu-CANF-Comb.

Compared to NPRC-targeted $^{64}$Cu-CANF-Comb, without the conjugation of CANF peptide, the non-targeted $^{64}$Cu-Comb showed significantly lower tracer accumulation at the injury site at TP 1 (1.99 ± 0.88, $p<0.0001$, n=6). Moreover, no statistical difference was detected between tracer accumulations at the injured and sham-operated (1.63 ± 0.29, n=6) arteries

with the non-targeted $^{64}$Cu-Comb, consistent with NPRC receptor mediated uptake of the targeted $^{64}$Cu-CANF-Comb at the injured sites (Figure 2 F, G).

In contrast to the $^{64}$Cu-DOTA-CANF peptide tracer uptake acquired in the same rabbit model at the same time point, the $^{64}$Cu-CANF-Comb nanoparticle showed more than double the tracer accumulation on the injured artery, possibly due to extended blood circulation (Figure S1) and increased targeting capability.[21] Additionally, as we reported previously,[23] upon binding of $^{64}$Cu-CANF-Comb to NPRC receptors expressed on the cell surface, the nanoparticles are rapidly internalized, and the receptors recycled back to the cell surface to bind additional circulating nanoparticles in blood. This allows for cumulative tracer uptake at the injury site and enhancement of the target-to-background ratio,[21, 24] indicating the advantage of the as-developed nanoprobe for NPRC receptor targeting in atherosclerosis.

PET imaging with $^{64}$Cu-CANF-Comb was also performed at time points 2 and 3 (after angioplasty) to evaluate plaque progression. As shown in Figure 3, significant tracer uptake was detected in the injured arteries relative to the low uptake displayed in sham-operated arteries at both time points. Quantitative uptake analysis showed gradually decreased tracer uptake at the injury site (4.35±0.96 at TP 2 and 4.07±1.07 at TP 3, n=8 for both) compared to the data acquired at TP 1, possibly due to the reduced cellularity in the neointima of plaques as we previously reported.[21] Nevertheless, at each time point, $^{64}$Cu-CANF-Comb showed significantly higher uptake at the injury sites compared to those acquired with non-targeted $^{64}$Cu-Comb, confirming the targeting specificity of $^{64}$Cu-CANF-Comb.

Additionally, $^{18}$F-FDG was used for plaque imaging in the atherosclerotic rabbits to compare with $^{64}$Cu-CANF-Comb. As shown in Figure 4A, comparable PET signals were present in sham operated and injured arteries at time point 1. Though quantitative data analysis showed that $^{18}$F-FDG accumulation in the injured arteries was higher than in the sham arteries at all three time points, the differences were not statistically significant (Figure 4B). Moreover, the injury/sham SUV ratios of $^{64}$Cu-CANF-Comb were significantly higher than those acquired with non-targeted $^{64}$Cu-Comb or $^{18}$F-FDG at all three time points, indicating the advantage of $^{64}$Cu-CANF-Comb for NPRC targeted imaging of advanced atherosclerotic lesions.

## Characterization of NPRC expression on atherosclerotic plaques in rabbits

Histopathological characterization of a representative injured rabbit artery collected 4 weeks after air desiccation showed the formation of primary neointima containing increased numbers of foam cells and smooth muscle cells compared to intact internal elastic lamina shown in the sham-operated artery (Figure 5), consistent with our previous report.[21] Immunofluorescent staining showed dense expression of NPRC receptor positive cells in the neointima of the plaque in contrast to the lower signal confined to the endothelium (and internal elastic lamina) observed in the sham artery, further confirming the PET imaging data. Additionally, Western blotting confirmed a stronger signal in the injured artery (Figure 5H) relative to the sham-operated artery (Figure 5D).

### Characterization of NPRC expression on plaque specimens from patients undergoing CEA

To assess the translational potential of $^{64}$Cu-CANF-Comb nanoparticles for NPRC imaging in patients with atherosclerosis, human plaque specimens collected during carotid endarterectomy (CEA) were analyzed for expression of NPRC receptor and *ex vivo* binding of $^{64}$Cu-CANF-Comb to the tissue. As shown in Figure 6A, H&E and VVG staining showed a large lipid-rich necrotic core, with some regions of thinned fibrous cap. Immunofluorescent staining showed dense expression of NPRC in the deep intima of the plaque. Autoradiography with $^{64}$Cu-CANF-Comb displayed significant tracer binding to the plaque in a pattern similar to the expression of NPRC receptor, consistent with binding to the receptor. Competitive receptor blocking using an excess of non-radiolabeled CANF-Comb showed a significant decrease in signal on the specimen, consistent with binding specificity of $^{64}$Cu-CANF-Comb for NPRC receptors in the human atherosclerotic plaque.

## CONCLUSIONS

In summary, we have assessed the imaging efficiency and translational potential of NPRC receptors targeted with $^{64}$Cu-CANF-Comb nanoparticles for imaging complex atheromatous plaques using a rabbit double injury-induced atherosclerosis model and *ex vivo* human CEA specimens. The modular design and construction of the CANF-Comb assembly provides accurate control over the physicochemical properties for *in vivo* plaque imaging. The extended blood circulation, improved binding efficiency, and rapid internalization/recycling kinetics of NRPC receptors result in improved imaging sensitivity and specificity as demonstrated in the rabbit model of advanced atherosclerosis. The biological characterization of NRPC receptors in the injured arteries using immunostaining and Western blot further confirmed the upregulation of NPRC receptor in the developing plaque and PET imaging results. *Ex vivo* exposure of human CEA specimens to $^{64}$Cu-CANF-Combs demonstrated binding to NPRC receptors, illustrating the potential of this nanoprobe for human plaque imaging translation.

## EXPERIMENTAL SECTION

### Materials.

Chemicals were purchased from Sigma-Aldrich (St. Louis, MO) and used without further purification unless stated. CANF peptide (98%, H-Arg-Ser-Ser-Cys-Phe-Gly-Gly-Arg-Ile-Asp-Arg-Ile-Gly-Ala-Cys-NH2) was obtained from CPC Scientific (Sunnyvale, CA) by custom synthesis. Dioxopyrrolidin-1-yl pent-4-ynoate was purchased from Annova Chemical Inc (San Diego, CA), poly(ethylene glycol)-$N_3$ (PEG-$N_3$) from Nanocs Inc. (New York, NY), poly(ethylene glycol) monomethyl ether from Polymer Source (Dorval, QC, CAN) and 1,4,7,10-tetraazacyclododecane-1,4,7-tris(t-butyl acetate) (DOTA-t-Bu-ester) from Macrocyclics (Dallas, TX). Amicon Centriplus centrifugal filtration tubes (MW cut-off = 30,000; 50,000) were purchased from Millipore (Billerica, MA). $^{64}$Cu (half-life = 12.7 h, $\beta^+$ = 17%, $\beta^-$ = 40%) was prepared on the Washington University Medical School CS-15 Cyclotron by the $^{64}$Ni(p,n)$^{64}$Cu nuclear reaction at a specific activity of 1.85 GBq – 7.4 GBq/μg (end of bombardment). The buffers used for $^{64}$Cu-labeling were treated with

Chelex-100 resin (Bio-Rad Laboratories, Hercules, CA) before use. 2,5-HiTrap Desalting columns (5 mL) were purchased from GE Healthcare Biosciences (Piscataway, NJ).

## Instrumentation

Gel permeation chromatography (GPC) was carried out on a Waters (Millford, MA) chromatograph equipped with a Waters Alliance high pressure liquid chromatography (HPLC) system pump (2695 Separation Module) and four Visco Gel I-Series columns from Viscotek (dimensions = 7.8 mm × 30 cm). Detection was provided by a Waters 2414 differential refractometer and N,N-dimethyl formamide (DMF) with 0.1 % LiBr used as the mobile phase. Copolymer chromatograms were run at room temperature and calibrated to poly(methyl methacrylate) (PMMA) standards. Dynamic light scattering (DLS) was performed on a Wyatt Technology (Goleta, CA) DynaPro NanoStar™ at room temperature. Data was collected on 0.1 wt% aqueous nanoparticle solutions filtered through a 0.2 μm filter. Zeta potential measurements were acquired on a Malvern Zetasizer (Zetasizer Nano ZS ZEN3600, Westborough, MA). A Bioscan 200 imaging scanner (Bioscan, Washington, DC) was used to read the instant thin layer chromatography (ITLC) plates (Pall ITLC-SG plates, VWR International, Batavia, IL). Fast protein liquid chromatography (FPLC) and radio-FPLC were performed using an ÄKTA FPLC system (GE Healthcare Biosciences, Pittsburgh, PA) equipped with a Beckman 170 Radioisotope Detector (Beckman Instruments, Fullerton, CA).

## Synthetic Procedures

Experimental procedures for the synthesis of S-methoxycarbonylphenylmethyl dithiobenzoate reversible addition-fragmentation chain-transfer (RAFT) agent;[25] macro- and small molecule monomers, polyethylene glycol methacrylate (PEGMA), DOTA methacrylate (DOTA-MA) and CANF-PEG methacrylate (CANF-PEGMA); CANF-comb copolymers; and nanoparticles were adopted from previously published work with minor modifications.[20, 26]

Synthesis of CANF-acetylene was carried out as previously reported with the following modification: 2,5-Dioxopyrrolidin-1-yl pent-4-ynoate was used in the place of 4-pentynoic anhydride. CANF-PEGMA was prepared as previously reported with the following modification to the purification: the product was washed with a 0.01 M aqueous ethylenediaminetetraacetic acid (EDTA) solution containing 0.02 M NaOH (× 4) and Milli-Q water (× 10). Comb copolymers were synthesized as follows: PEGMA, 5.0 kDa (205 mg, 0.041 mmol), CANF-PEGMA 5.0 kDa (100 mg, 0.015 mmol), methyl methacrylate (MMA) (51.1 mg, 0.51 mmol), azobisisobutyronitrile (AIBN) (0.069 mg, 0.00042 mmol), DOTA-MA (22.2 mg, 0.032 mmol), and RAFT agent (0.33 mg, 0.0011 mmol) were added to a glass vial and dissolved in DMF (1.99 g). AIBN, DOTA-MA and the RAFT agent were all added to the vial as DMF stock solutions. The solution was transferred to a 5 mL Schlenk flask and degassed by three freeze-pump-thaw cycles followed by heating to 70 °C for 120 h. Following polymerization, the solution was diluted with DMF, transferred to four 15 mL Amicon Centriplus tubes (MW cut-off = 50,000) and extensively washed with DMF until complete removal of monomers was observed by GPC. The copolymer was then washed with MilliQ water (× 5) and freeze-dried to give the desired graft copolymer as a white

powder (yield ~68 mg); Mn = 205 kDa, PDI = 1.20 (GPC-DMF, PMMA standards). The non-targeted comb copolymer (0% CANF) was synthesized with 0.056 mmols of PEGMA and no CANF-PEGMA monomer.

Deprotection and assembly of the CANF-combs into nanoparticles was carried out by the following protocol: After deprotection of the t-butyl esters of the DOTA groups, the freeze-dried comb copolymer was dissolved in DMSO (1 wt %) and heated to 50 °C until fully dissolved. The solution was cooled to room temperature, and an equal volume of Milli-Q water was added while stirring. To remove DMSO, the solution was transferred to two Amicon Centriplus (MW cut-off = 30,000) centrifugal filtration tubes and concentrated, followed by re-dilution with Milli-Q water until the DMSO content was less than 0.5 mg / mL by $^{1}$H NMR. The resultant particles were characterized by DLS, rediluted to 10 mg/mL and stored at −20 °C.

## $^{64}$Cu Radiolabeling of CANF-Comb and Comb Nanoparticles

The radiolabeling of CANF-comb and comb nanoparticles was as reported previously.[20, 26] Briefly, the nanoparticles (5 μg, 5 pmol) were incubated with 185 MBq $^{64}$Cu in 100 μL of a 0.1 M pH 5.5 ammonium acetate buffer at 80°C for 1 h. After adding 5 μL EDTA (10 mM in 50 mM pH 7.4 phosphate buffer) to remove any non-specifically bound $^{64}$Cu from the nanoparticles, the $^{64}$Cu radiolabeled nanoparticles were separated from $^{64}$Cu-EDTA with a 2 mL zeba spin desalting column. A 2 μL aliquot of the purified nanoparticles was spotted on glass microfiber chromatography paper impregnated with silica gel and developed in a buffer composed of methanol and 10% ammonium acetate (volume ratio = 1:1). After separation, the radiochemical purity (RCP) of the $^{64}$Cu radiolabeled nanoparticles was measured by radioactive thin layer chromatography (Radio-TLC, Washington, DC) to ensure the RCP was 95% or greater prior to *in vivo* studies.

## Animal Preparations to Induce Atherosclerotic-like Lesions

All animal studies were performed in compliance with guidelines set forth by the National Institutes of Health Office of Laboratory Animal Welfare and approved by the Washington University Institutional Animal Care and Use Committee. Atherosclerotic-like arterial lesions were induced in the right femoral artery of male New Zealand White rabbits by air desiccation, followed by angioplasty at a later time point (TP), as reported previously.[21] The left femoral artery was surgically exposed, but remained uninjured as a sham control.

Briefly, rabbits were fed a 0.25% cholesterol-enriched diet (Purina, St. Louis, MO) throughout the study, and elevated serum cholesterol (˃200 mg/dL) was confirmed at the time of vessel injury. The right femoral artery was exposed aseptically through a longitudinal skin incision, and lidocaine was applied topically to prevent spasm. A 1- to 2-cm segment of the vessel was isolated between air-tight ligatures, and small branches were ligated with suture. A 27-gauge needle was used to puncture the isolated segment proximally as a vent. A second 27-gauge needle was inserted distally into the segment, and nitrogen gas was passed through the vessel at a flow rate of 80 mL/min for 8 min to dry and cause sloughing of the endothelium. The segment was then flushed with saline, and the ligatures were released to restore blood flow, with gentle pressure applied to the puncture sites for a

few minutes to maintain hemostasis. The skin incision was closed, and the animal was allowed to recover from anesthesia. Four to six weeks after the air desiccation–induced injury, the lesion site and extent of stenosis in the femoral artery were identified by angiography obtained using a 4-French guide catheter introduced through a carotid arterial cutdown and advanced to the distal aorta. Heparin (100 U/kg, intravenously) was given to prevent clot formation in the catheters. A 0.014-cm guidewire was then advanced across the lesion, and the guide catheter was removed. A 2.0–2.5 × 20 mm coronary angioplasty balloon was advanced over the guidewire, and the site of stenosis was dilated with three, 30-s balloon inflations of 6–8 atmospheres, with 1 min between inflations. After reinjuring the lesion site, patency of the femoral artery was confirmed by an angiogram through the angioplasty catheter before the catheter was removed. The carotid was ligated, the skin incision closed, and the animal was allowed to recover from anesthesia.

## Rabbit PET Imaging Protocol

The experimental design is schematized in figure 1. To determine the tracer uptake, 12 rabbits were imaged with PET (focus 220, Siemens Healthcare) at 4–6 weeks after the air-desiccation-induced injury (time point 1, TP 1). Eight rabbits were imaged again at 4–6 weeks after balloon overstretch-induced injury (TP 2), and 4 rabbits coming from TP 2 were imaged with PET at 8 weeks after the second injury (TP 3). For each rabbit, approximately 55 ± 8 MBq of purified $^{64}$Cu-CANF-Comb was injected through a catheter in an ear vein. PET imaging was performed at 24 h post injection (60 min static scan). For competitive receptor blocking studies, rabbits (n=4) at TP 1 were co-injected with $^{64}$Cu-CANF-Comb and an excess of non-radiolabled CANF-Comb (CANF-Comb:$^{64}$Cu-CANF-Comb molar ratio = 100:1) and scanned 24 h later. Tissue specimens of injured and sham-operated arteries were collected at each TP for histology and immunohistochemistry. PET images were processed using the manufacturer's software (ASI Pro). The tracer uptake in the region of interest (ROI) was calculated as standardized uptake values (SUVs). $^{18}$F-FDG (100 ± 20 MBq) PET was also performed at 1 h post injection (20 min static scan) in the rabbits at the three time points post injury to compare with the data obtained using $^{64}$Cu-CANF-Comb.

To compare the blood retention between $^{64}$Cu-CANF-Comb and $^{64}$Cu-DOTA-CANF peptide tracer,[21] 10–15 blood samples (5–10 μL/sample) were drawn from the rabbit's ear vein catheter within the first minute post tracer injection. Additional blood samples were collected every 5 minutes. All samples were counted in a gamma counter to calculate the blood retention of the tracers.

## NPR-C Protein Assay by Western Blot and Histopathology of Injured Rabbit Femoral Arteries

For Western blotting of NPRC protein in vessel extracts, injured and sham arteries were dissected, rinsed with saline, and frozen at −80C. The frozen artery was transferred to a pre-chilled 1.5 ml microcentrifuge tube and 500 μL of RIPA EDTA protease inhibitor was added. The tissue was homogenized on ice using a tissue homogenizer followed by sonication. Samples were then incubated for 30min on ice, centrifuged for 30 min at 12,000 RPM at 4°C, and the supernatant transferred to a new microcentrifuge tube. If any particulate was observed, the centrifugation was repeated. Protein in the sample supernatant

was determined using the bicinchoninic acid assay. Samples were separated by electrophoresis on a Mini-Protean TGX 10%, 15 well gel in a BioRad MiniProtean II Western Apparatus System. Running buffer was prepared and added to the apparatus according to the instructions. Tissue homogenate samples were thawed and re-heated to 70°C followed by centrifugation and vortex mixing. Samples (15 μL) were loaded into the wells on the gel together with a True Blue protein ladder on each end of the gel. The gel was run at 60 V for 10 min and then 100 V for 40 min or until the loading dye reached the bottom of the gel. The gel was carefully removed and placed in a transfer cassette overlaid with Immun-Blot PVDF membrane previously equilibrated in methanol and transfer buffer. The transfer was carried out at 80V for 90 min in the cold. Ponceau staining confirmed transfer of protein from the gel to the membrane. The membrane was washed in $dH_2O$, blocked with 5% nonfat dry milk in TBS for 1h at room temperature, washed with TBS, and incubated with NPR-C antibodies (human IgG, mouse monoclonal at 1:1000 in TBS + 5% BSA) overnight in the cold. After washing with TBS, the membrane was incubated in 1: 10,000 goat-anti-mouse secondary antibody for 1 h at RT. The membrane was exposed to chemiluminescence reagents for 1 minute, blotted off and the membrane placed in an X-ray cassette with film in a dark room to expose for 30 min. The membrane was then probed for β-actin as a protein control for 10 sec. Fold increase of NPR-C from non-injured to injured at different times were calculated.

After radioactive decay, rabbit artery specimens were fixed in fresh 4% paraformaldehyde overnight, embedded in paraffin, and cut in cross-section at a thickness of 5 μm for histologic examination and immunofluorescence. Histologic examination was performed using hematoxylin and eosin (H&E) and Verhoeff's Van Gieson (VVG) staining. For immune staining, sections were deparaffinized in a graded series of xylene and rehydrated through a series of graded alcohols into PBS. Antigen retrieval was done by boiling the sections in buffer (pH 6.2 Diva Decloaker, 1x). They were then blocked in 10% donkey serum for 1 h to prevent nonspecific binding and incubated at 4 °C in primary antibody (anti-NPRC, Genway Biotech, 1:00) or control IgG (anti-mouse IgG, Abcam, 1:100). FITC-conjugated, anti-mouse secondary antibody was applied (Jackson Laboratories) for 1 h at room temperature, and sections were washed in PBS, mounted in DAPI mounting medium (Vector Laboratories), and imaged using a Leica fluorescent microscope system.

### Immunostaining of human tissues

Human carotid endarterectomy specimens were placed in sterile saline in the operating room and fixed in 10% formalin overnight, embedded in paraffin, and sectioned at a thickness of 5 μm for immunohistochemistry. Whole specimen histologic evaluations were performed using H&E and pentachrome staining to examine tissue architecture. Paraffin embedded sections were deparaffinized in xylenes and rehydrated through a series of graded alcohols into PBS. Tissues were processed for antigen retrieval by boiling in buffer (pH 6.2 Diva Decloaker, 1×). They were blocked in blocking serum for 1 h to prevent nonspecific binding (Vectastain; Vector Laboratories). The sections were then incubated overnight at 4 °C with primary antibody (anti-NPRC, Genway Biotech, 1:100) or control IgG (anti- mouse IgG, Abcam, 1:100). Secondary antibody was applied (Vector Laboratories) and color development was achieved through alkaline phosphatase to yield a blue color. The sections

were counterstained with Nuclear Fast Red (pink), and imaged using a Leica light microscope system.

### Autoradiography.

Fixed human CEA tissue sections were deparaffinized in Citrasolv and rehydrated through a series of graded alcohols and into PBS. The slides were incubated with $^{64}$Cu-CANF-Comb (0.925 MBq) for 15 min. Slides were extensively washed with water and then covered by a phosphor-imaging film plate and exposed overnight at −20 °C prior to imaging with a Molecular Dynamics Storm Imager 840. For blocking studies, similar procedures were performed in the presence of non-radiolabeled CANF-Comb in excess amount (CANF-Comb: $^{64}$Cu-CANF-Comb molar ratio=100:1).

### Statistical Analysis

Data are described as the mean ± standard deviation. Group comparisons were made using the one-way ANOVA. The significance level in all tests was $p \leq 0.05$. GraphPad Prism v. 6.04 (La Jolla, CA) was used for all statistical analyses.

## Supplementary Material

Refer to Web version on PubMed Central for supplementary material.

## ACKNOWLEDGMENT AND DISCLOSURES

This work was supported by a Program of Excellence in Nanotechnology (HHSN268201000046C) from the National Heart, Lung and Blood Institute of the National Institutes of Health. The characterization of nanoparticles was performed in the Central Facilities of the UCSB Materials Research Laboratory supported by the MRSEC Program of the National Science Foundation under award no. DMR-1720256. The authors have no relevant conflicts of interest pertaining to this research.

We thank Pamela Baum for assistance with the atherosclerosis preparation and angioplasty in rabbits; Nicole Fettig, Margaret Morris, Amanda Roth, Lori Strong, and Ann Stroncek for their assistance with the imaging studies in animals; and Tom Voller, Evelyn Madrid, and Paul Eisenbeis, for $^{64}$Cu production, and Christian Roh for assistance with the Western blotting of tissue for NPRC. We also thank Dr. Richard Pierce for helpful discussion and comments about the data.

## REFERENCES

(1). Libby P Inflammation in atherosclerosis. Arterioscler. Thromb. Vasc. Biol 2012, 32 (9), 2045–2051. [PubMed: 22895665]

(2). Kasikara C; Doran AC; Cai B; Tabas I The role of non-resolving inflammation in atherosclerosis. J. Clin. Invest 2018, 128 (7), 2713–2723. [PubMed: 30108191]

(3). Williams JW; Elvington A; Ivanov S; Kessler S; Luehmann H; Baba O; Saunders BT; Kim KW; Johnson MW; Craft CS; Choi JH; Sorci-Thomas MG; Zinselmeyer BH; Brestoff JR; Liu Y; Randolph GJ Thermoneutrality but Not UCP1 Deficiency Suppresses Monocyte Mobilization Into Blood. Circ. Res 2017, 121 (6), 662–676. [PubMed: 28696252]

(4). Kazuma SM; Sultan D; Zhao Y; Detering L; You M; Luehmann HP; Abdalla DS; Liu Y Recent Advances of Radionuclide-Based Molecular Imaging of Atherosclerosis. Curr. Pharm. Des 2015, 21 (36), 5267–5276. [PubMed: 26369676]

(5). Libby P; Ridker PM; Hansson GK Progress and challenges in translating the biology of atherosclerosis. Nature 2011, 473 (7347), 317–325. [PubMed: 21593864]

(6). Heidenreich PA; Trogdon JG; Khavjou OA; Butler J; Dracup K; Ezekowitz MD; Finkelstein EA; Hong Y; Johnston SC; Khera A; Lloyd-Jones DM; Nelson SA; Nichol G; Orenstein D; Wilson

PW; Woo YJ Forecasting the future of cardiovascular disease in the United States: a policy statement from the American Heart Association. Circulation 2011, 123 (8), 933–944. [PubMed: 21262990]

(7). Magnoni M; Ammirati E; Camici PG Non-invasive molecular imaging of vulnerable atherosclerotic plaques. J. Cardiol 2015, 65 (4), 261–269. [PubMed: 25702846]

(8). Sanz J; Fayad ZA Imaging of atherosclerotic cardiovascular disease. Nature 2008, 451 (7181), 953–957. [PubMed: 18288186]

(9). Wildgruber M; Swirski FK; Zernecke A Molecular Imaging of Inflammation in Atherosclerosis. Theranostics 2013, 3 (11), 865–884. [PubMed: 24312156]

(10). Andrews JPM; Fayad ZA; Dweck MR New methods to image unstable atherosclerotic plaques. Atherosclerosis 2018, 272, 118–128. [PubMed: 29602139]

(11). Tarkin JM; Joshi FR; Rajani NK; Rudd JH PET imaging of atherosclerosis. Future Cardiol. 2015, 11 (1), 115–131. [PubMed: 25606707]

(12). Nie X; Laforest R; Elvington A; Randolph GJ; Zheng J; Voller T; Abendschein DR; Lapi SE; Woodard PK PET/MRI of Hypoxic Atherosclerosis Using 64Cu-ATSM in a Rabbit Model. J. Nucl. Med 2016, 57 (12), 2006–2011. [PubMed: 27390157]

(13). Perez-Medina C; Hak S; Reiner T; Fayad ZA; Nahrendorf M; Mulder WJM Integrating nanomedicine and imaging. Philos. Trans. A Math. Phys. Eng. Sci 2017, 375 (2107).

(14). Noukeu LC; Wolf J; Yuan B; Banerjee S; Nguyen KT Nanoparticles for Detection and Treatment of Peripheral Arterial Disease. Small 2018, 14 (32), e1800644. [PubMed: 29952061]

(15). Keliher EJ; Ye YX; Wojtkiewicz GR; Aguirre AD; Tricot B; Senders ML; Groenen H; Fay F; Perez-Medina C; Calcagno C; Carlucci G; Reiner T; Sun Y; Courties G; Iwamoto Y; Kim HY; Wang C; Chen JW; Swirski FK; Wey HY; Hooker J; Fayad ZA; Mulder WJ; Weissleder R; Nahrendorf M Polyglucose nanoparticles with renal elimination and macrophage avidity facilitate PET imaging in ischaemic heart disease. Nat. Commun 2017, 8, 14064. [PubMed: 28091604]

(16). Bejarano J; Navarro-Marquez M; Morales-Zavala F; Morales JO; Garcia-Carvajal I; Araya-Fuentes E; Flores Y; Verdejo HE; Castro PF; Lavandero S; Kogan MJ Nanoparticles for diagnosis and therapy of atherosclerosis and myocardial infarction: evolution toward prospective theranostic approaches. Theranostics 2018, 8 (17), 4710–4732. [PubMed: 30279733]

(17). Liu Y; Pressly ED; Abendschein DR; Hawker CJ; Woodard GE; Woodard PK; Welch MJ Targeting angiogenesis using a C-type atrial natriuretic factor-conjugated nanoprobe and PET. J. Nucl. Med 2011, 52 (12), 1956–1963. [PubMed: 22049461]

(18). Perez-Medina C; Binderup T; Lobatto ME; Tang J; Calcagno C; Giesen L; Wessel CH; Witjes J; Ishino S; Baxter S; Zhao Y; Ramachandran S; Eldib M; Sanchez-Gaytan BL; Robson PM; Bini J; Granada JF; Fish KM; Stroes ES; Duivenvoorden R; Tsimikas S; Lewis JS; Reiner T; Fuster V; Kjaer A; Fisher EA; Fayad ZA; Mulder WJ *In vivo* PET Imaging of HDL in Multiple Atherosclerosis Models. JACC Cardiovasc. Imaging 2016, 9 (8), 950–961. [PubMed: 27236528]

(19). Beldman TJ; Senders ML; Alaarg A; Perez-Medina C; Tang J; Zhao Y; Fay F; Deichmoller J; Born B; Desclos E; van der Wel NN; Hoebe RA; Kohen F; Kartvelishvily E; Neeman M; Reiner T; Calcagno C; Fayad ZA; de Winther MPJ; Lutgens E; Mulder WJM; Kluza E Hyaluronan Nanoparticles Selectively Target Plaque-Associated Macrophages and Improve Plaque Stability in Atherosclerosis. ACS Nano 2017, 11 (6), 5785–5799. [PubMed: 28463501]

(20). Woodard PK; Liu Y; Pressly ED; Luehmann HP; Detering L; Sultan DE; Laforest R; McGrath AJ; Gropler RJ; Hawker CJ Design and Modular Construction of a Polymeric Nanoparticle for Targeted Atherosclerosis Positron Emission Tomography Imaging: A Story of 25% (64)Cu-CANF-Comb. Pharm Res. 2016, 33 (10), 2400–2410. [PubMed: 27286872]

(21). Liu Y; Abendschein D; Woodard GE; Rossin R; McCommis K; Zheng J; Welch MJ; Woodard PK Molecular imaging of atherosclerotic plaque with 64Cu-labeled natriuretic peptide and PET. J. Nucl. Med 2010, 51 (1), 85–91. [PubMed: 20008978]

(22). Zayed MA; Harring SD; Abendschein DR; Vemuri C; Lu D; Detering L; Liu Y; Woodard PK Natriuretic Peptide Receptor-C is Up-Regulated in the Intima of Advanced Carotid Artery Atherosclerosis. J. Med. Surg. Pathol 2016, 1 (3).

(23). Luehmann HP; Pressly ED; Detering L; Wang C; Pierce R; Woodard PK; Gropler RJ; Hawker CJ; Liu Y PET/CT imaging of chemokine receptor CCR5 in vascular injury model using targeted nanoparticle. J. Nucl. Med 2014, 55 (4), 629–634. [PubMed: 24591489]

(24). Potter LR Natriuretic peptide metabolism, clearance and degradation. Febs j. 2011, 278 (11), 1808–1817. [PubMed: 21375692]

(25). Perrier S; Takolpuckdee P; Westwood J; Lewis DM Versatile Chain Transfer Agents for Reversible Addition Fragmentation Chain Transfer (RAFT) Polymerization to Synthesize Functional Polymeric Architectures. Macromolecules 2004, 37 (8), 2709–2717.

(26). Pressly ED; Pierce RA; Connal LA; Hawker CJ; Liu Y Nanoparticle PET/CT imaging of natriuretic peptide clearance receptor in prostate cancer. Bioconjugate chem. 2013, 24 (2), 196–204.

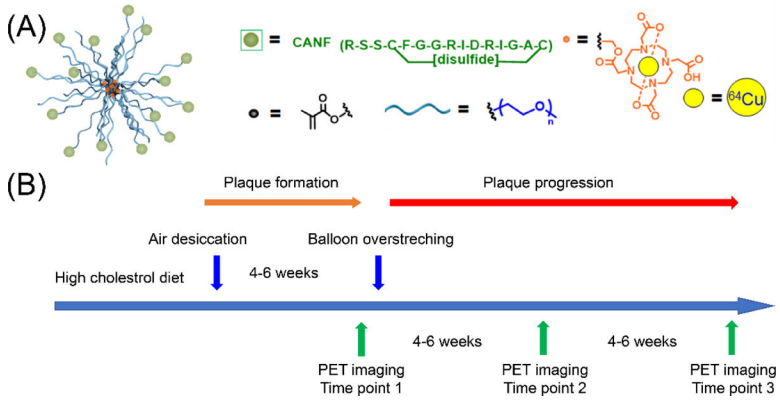


**Figure 1.**

Illustration of (A) CANF-Comb nanoparticle design and (B) rabbit atherosclerosis model timeline.

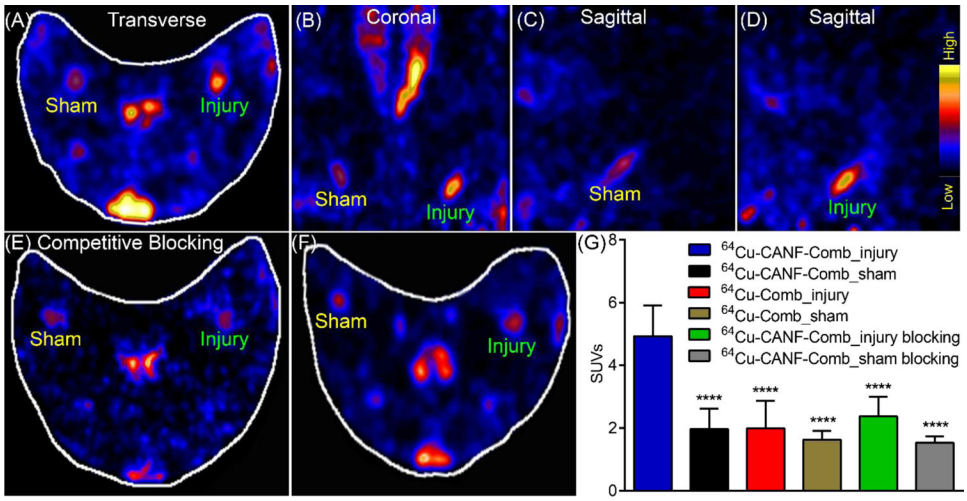


**Figure 2.**

Representative PET images 24h post-IV injection of $^{64}$Cu-CANF-Comb in a rabbit 4 weeks after air desiccation-induced injury and quantitative data analysis. (A) transverse view, (B) coronal view, (C) sagittal view of sham-operated artery, (D) sagittal view of injured-artery, (E) competitive blocking of $^{64}$Cu-CANF-Comb binding by co-injection of non-radiolabeled CANF-Comb (CANF-Comb: $^{64}$Cu-CANF-Comb molar ratio= 100:1), (F) transverse PET image of non-targeted $^{64}$Cu-Comb, (G) quantitative uptake analysis. **** $p<0.001$, compared to the tracer uptake acquired in the injured artery with $^{64}$Cu-CANF-Comb. n=12 for $^{64}$Cu-CANF-Comb, n=6 for $^{64}$Cu-Comb, n=4 for $^{64}$Cu-CANF-Comb blocking.

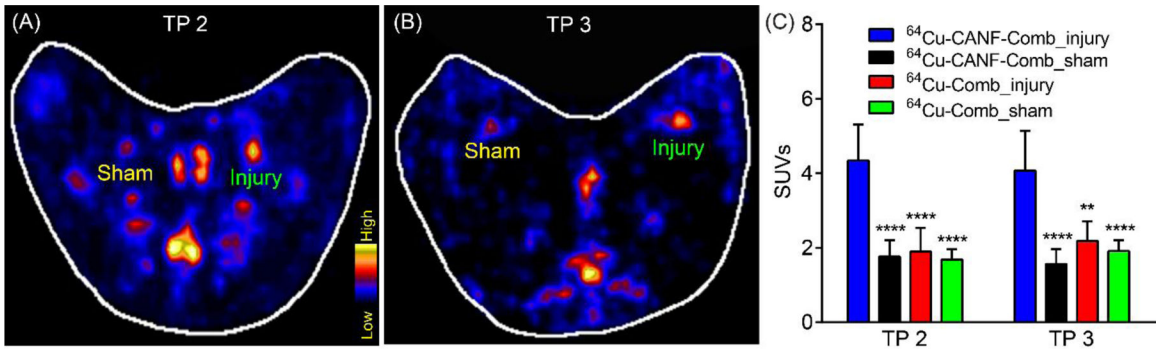


**Figure 3.**

Representative $^{64}$Cu-CANF-Comb PET images at 4 weeks (A, TP 2) and 8 weeks (B, TP 3) after balloon overstretching of the air dessicated segment in rabbit femoral arteries from two rabbits, (C) quantitative uptake analysis. **, $p<0.01$, ****, $p< 0.001$, compared to the tracer uptake acquired in the injured artery with $^{64}$Cu-CANF-Comb. n=8 for $^{64}$Cu-CANF-Comb, n=4 for $^{64}$Cu-Comb at each time point.

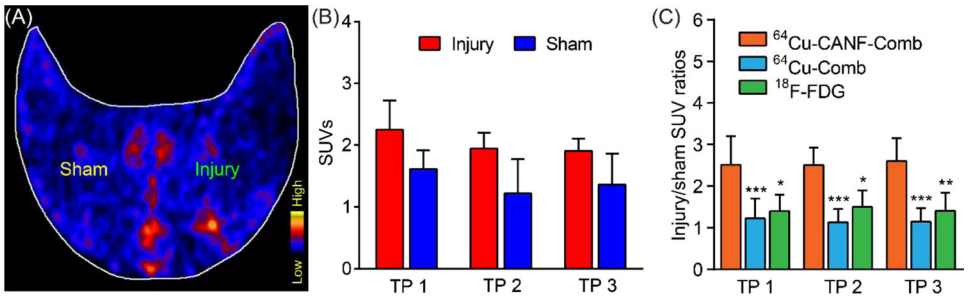


**Figure 4.**

(A) Representative $^{18}$F-FDG rabbit PET images at 4 weeks post air desiccation injury of femoral arteries, (B) quantitative uptake analysis at three time points (TP), (C) comparison of injury/sham uptake ratios among $^{64}$Cu-CANF-Comb, $^{64}$Cu-Comb and $^{18}$F-FDG at three time points. *, $p < 0.05$, **, $p < 0.01$, ***, $p < 0.005$, n=4 for $^{18}$F-FDG at all time points.

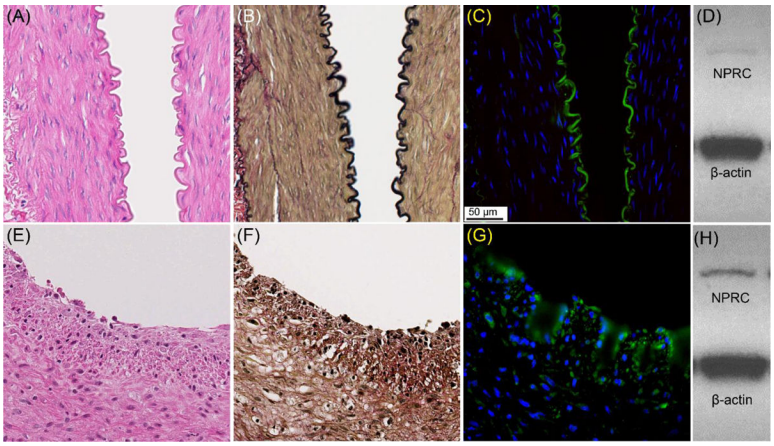


**Figure 5.**

Histopathologic characterization and NPRC expression in intact, sham-operated (A-D) and air dessication-induced injured (E-H) rabbit femoral arteries 4 weeks after injury. A. H&E stain, B. VVG stain, C. NPRC immunofluorescent stain(green), and D. Western blot E. H&E stain, (F) VVG, G. immunofluorescent stain of NPRC (green), and (H) Western blot of injured artery. All images were at 40x.

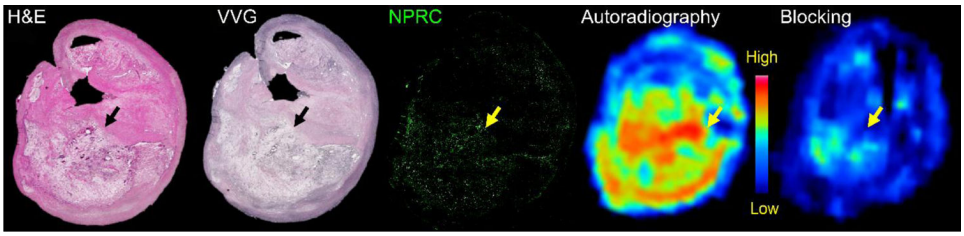


**Figure 6.**

*Ex vivo* characterization of a human plaque specimen collected after carotid endarterectomy. H&E and VVG staining showed a large lipid-rich, necrotic core in the deep intima (arrow), with some regions of thinned fibrous cap. Immunofluorescent staining showed upregulation of NPRC receptor (green below yellow arrow) on the plaque. Autoradiography of *ex vivo* specimen showed binding of $^{64}$Cu-CANF-Comb to the plaque in the area of expression of the NPRC receptor. Competitive receptor blocking showed decreased signal, demonstrating the specificity of $^{64}$Cu-CANF-Comb binding for NPRC.

**Table 1.**

Characterization of Comb and CANF-Comb polymers

| Polymer | $M_n$[a] | Đ[a] | Size (nm)[b] | ζ-Potential (mV) | # of CANF/ nanoparticle[c] | # of DOTA/ nanoparticle[c] | $^{64}$Cu radiolabeling specific activity (GBq/ nmol) |
|---|---|---|---|---|---|---|---|
| **Comb** | 220,000 | 1.25 | 21 | −32±3 | 0 | 105 | 5.0±1.0 |
| **CANF-Comb** | 205,000 | 1.20 | 14 | −2±1 | 35 | 105 | 4.0±1.0 |

[a] Determined by GPC in DMF, calibrated to PMMA standards ($gmol^{-1}$), Đ = $M_w/M_n$.

[b] Measured by dynamic light scattering.

[c] Predicted incorporation